Enhanced Support Recovery for PMU Measurements Based on Taylor–Fourier Compressive Sensing Approach

Guglielmo Frigo, *Member, IEEE*, Paolo Attilio Pegoraro, *Senior Member, IEEE*, and Sergio Toscani, *Senior Member, IEEE*

***Abstract*— Modern distribution networks are characterized by higher distortion and faster variability of voltages and currents. Accurate synchrophasor, frequency, and rate-of-change-of-frequency measurements thus ask for new techniques trying to reduce latency while limiting the impact of spurious components. In this respect, Taylor–Fourier multifrequency approach is a good candidate for phasor measurement units intended for distribution system applications. In this present article, we propose an enhanced version of this approach based on the joint application of window functions and iterative support refinement by means of the phasor first-order derivative. The performance of the algorithm is thoroughly characterized through extensive numerical simulation of nonstandard test conditions that reproduce the challenges of real-world scenarios, with fundamental dynamics superimposed on interfering tones. The reported results confirm the enhanced spectral support recovery, resulting in a remarkable improvement of estimation accuracy.**

***Index Terms*— Coherence, compressed sensing, phasor measurement units (PMUs), power system harmonics, rate-of-change-of-frequency (ROCOF), spectral support, Taylor–Fourier multifrequency, window function.**

I. Introduction

In RECENT years, distribution networks are experiencing a significant transformation; the traditional generation paradigm based on synchronous generators is accompanied by the integration of renewable energy sources (RESs). The interconnection of such resources relies on dedicated converters, whose power electronic circuitry switches at high frequency and produces nonnegligible harmonic and interharmonic disturbances [1]. These components may not be canceled by the analog front end of many instruments and thus cause significant errors in the measurement results. Moreover, this novel paradigm reduces the overall rotating inertia and makes the network more vulnerable against transient events and fast dynamics, also at the fundamental frequency [2].

In order to address this challenging scenario, many monitoring and control applications have been set up to update periodically the network state and identify possible anomalies or faults [3]. In a near future, these applications might rely also on the measurements of the so-called phasor measurement units (PMUs), i.e., instruments capable of estimating the synchrophasor, frequency, and rate-of-change-of-frequency (ROCOF) associated with the fundamental component at a reporting rate in the order of tens of frames-per-second (fps) [4]. In this regard, the recent IEC Std 60255-118-1 (IEC Std from here on) defines two performance classes, P and M, and the corresponding compliance limits in terms of total vector error (TVE), frequency error (FE), and ROCOF error (RFE) [5]. It is important to underline that the IEC Std refers to a transmission network scenario, where the penetration of RES and interface converters is negligible. Therefore, the IEC Std test conditions reflect a nearly stable operation with limited distortion due to harmonic or out-of-band (OoB) interference. Indeed, the rejection of spurious components is verified only in the presence of single harmonic or interharmonic tones, under steady-state conditions with nominal frequency and distortion levels not exceeding 10%.

In order to guarantee the reliability of such measurements also at the distribution level, it is necessary to test the PMUs and their estimation algorithms in more realistic scenarios [6]–[9]. In this sense, off-nominal and dynamic test conditions should be combined with the simultaneous presence of harmonic and interharmonic components [10].

To this end, the recent literature has investigated several different algorithmic approaches. Among them, the Taylor–Fourier filters (TFFs) prove to be a promising solution, as they allow for computing not only the synchrophasor but also its Taylor series expansion around the measurement instant [11], [12]. By including the high-order derivatives in the signal model, it is possible to account for time variations of the parameters of the fundamental component. More precisely, this allows for defining the instantaneous fundamental frequency and ROCOF as functions of the phase-angle first- and second-order derivatives. Such formulation has

Manuscript received 27 December 2021; revised 14 April 2022; accepted 5 May 2022. Date of publication 18 May 2022; date of current version 3 June 2022. The work of Paolo Attilio Pegoraro was supported in part by the Fondazione di Sardegna for the research project "IQSS—Information Quality aware and Secure Sensor networks for smart cities." The Associate Editor coordinating the review process was Dr. Manyun Huang. *(Corresponding author: Paolo Attilio Pegoraro.)*

Guglielmo Frigo is with the Laboratory of Electrical Energy and Power, Swiss Federal Institute of Metrology, 3003 Wabern bei Bern, Switzerland (e-mail: guglielmo.frigo@metas.ch).

Paolo Attilio Pegoraro is with the Department of Electrical and Electronic Engineering, University of Cagliari, 09123 Cagliari, Italy (e-mail: paolo.pegoraro@unica.it).

Sergio Toscani is with the Dipartimento di Elettronica, Informazione e Bioingegneria, Politecnico di Milano, 20133 Milan, Italy (e-mail: sergio.toscani@polimi.it).

Digital Object Identifier 10.1109/TIM.2022.3176275

a twofold advantage: enhance the estimation accuracy in dynamic conditions and minimize the reporting latency [13]. Unfortunately, the accuracy obtained with TFFs drastically degrades in the presence of interfering tones in the neighborhood of the fundamental component. For this reason, the compressive sensing Taylor–Fourier Multifrequency (CS-TFM) model applies a two-step procedure: first, a CS-based routine identifies the signal support (i.e., the set of most significant spectral components); then, a TFM model is defined considering the support. If properly identified, the interferences are minimized and the estimation accuracy is compliant with both P and M class requirements, even in the presence of interharmonic components at the boundaries of the PMU passband [14], [15].

The identification of the signal support is performed in the discrete Fourier transform domain by means of a dictionary, which in [16] consists of a set of Dirichlet kernels. This dictionary accounts for the spectral leakage contributions of a rectangular window: narrow and selective main lobe at the cost of high and slowly decaying sidelobes. This latter aspect tends to increase the interference coming from the negative frequency image components, especially if a reduced latency is envisioned [17].

The performance degradation is particularly noticeable in the RFE, as the second-order derivative term is particularly sensitive to spurious injections [18]. In the recent literature, several approaches have addressed the support recovery issue: a Kalman filter to exploit the regularity of consecutive estimates [19] or a peak detection routine for preliminary definition of the support cardinality [20]. In real-world conditions, though, these approaches still require a window length of at least five nominal cycles [21].

This article is the extension of [22], where the adoption of weighting to minimize leakage between spectral components was first proposed (compressive sensing weighted Taylor–Fourier multifrequency (CS-WTFM)). This idea corresponds to modifying the support identification dictionary in order to find the best tradeoff between precise location of spectral peaks and optimization of sidelobes decay. In particular, the Chebyshev window [23] proves to be a promising solution as it guarantees a reduction of the minimum window length and a remarkable enhancement of the estimation accuracy even in off-standard conditions. Based on these results, this article proposes a further improvement: the identification of the support is iteratively corrected by considering the phase-angle first derivative of the identified components (compressive sensing enhanced weighted Taylor–Fourier multifrequency (CS-EWTFM)). In this way, it is possible to check whether the selected set of frequencies is consistent with the frequency estimate of each component. The performance enhancement is confirmed by an extensive characterization in off-standard conditions. In particular, it is noticed that the proposed approach is more robust in the presence of fast dynamics and several interfering components.

This article is organized as follows. In Section II, we summarize the TFM theoretical foundations. Section III introduces CS-WTFM and the new CS-EWTFM and discusses their impact on support recovery. In Section IV, we characterize the algorithms performance in highly distorted test conditions. Finally, Section V provides some closing remarks and outlines future research.

II. Compressive Sensing Taylor–Fourier Multifrequency Approach

A. Taylor–Fourier Multifrequency Model

Let us consider an electrical signal $x(t)$ acquired with sampling interval T_s. The CS-TFM (TFM in the following) approach relies on the following model for a vector $\mathbf{x}$ made of an odd number N_w of samples of the aforementioned signal, centered on the time instant t_r:

$$\mathbf{x}(t_r) = \begin{bmatrix} x\left(t_r + \dfrac{N_w-1}{2}T_s\right) \\ \vdots \\ x(t_r) \\ \vdots \\ x\left(t_r - \dfrac{N_w-1}{2}T_s\right) \end{bmatrix} = \bar{\mathbf{B}}\bar{\mathbf{p}}(t_r) + \mathbf{r}$$
$$= \left[\bar{\Phi}_1\mathbf{A}_1 \cdots \bar{\Phi}_Q\mathbf{A}_Q \quad \bar{\Phi}_1^{\mathsf{H}}\mathbf{A}_1 \cdots \bar{\Phi}_Q^{\mathsf{H}}\mathbf{A}_Q\right]\bar{\mathbf{p}}(t_r) + \mathbf{r} \quad (1)$$

where $^{\mathsf{H}}$ is the Hermitian operator and overbars denote complex-valued quantities. Vector $\mathbf{r}$ expresses the model error at the different sampling instants, while $\bar{\mathbf{p}}$ includes all the unknown parameters of the model, and it can be written as

$$\bar{\mathbf{p}} = \left[\bar{X}_1^{(0)} \cdots \bar{X}_1^{(K_1)} \cdots \bar{X}_Q^{(0)} \cdots \bar{X}_Q^{(K_Q)} \quad \underline{X}_1^{(0)} \cdots \underline{X}_Q^{(K_Q)}\right] \quad (2)$$

where underbar indicates the conjugate of a complex number. Furthermore, $\bar{X}_l^{(k)}$ is the kth derivative of the harmonic or interharmonic phasor corresponding to the lth component having angular frequency $\omega_l = 2\pi f_l$; Q components are included in the model, each one with derivatives up to the order K_l. Their negative frequency images are always present since $x(t)$ is assumed to be real-valued. All the above quantities are referred to the same time instant t_r, which will be often omitted for a lighter notation. In order to fully define the model in (1), it is necessary to introduce

$$\bar{\Phi}_l = \bar{\Phi}(\omega_l) = \begin{bmatrix} e^{j\omega_l\frac{N_w-1}{2}T_s} & & & & \\ & \ddots & & & \\ & & 1 & & \\ & & & \ddots & \\ & & & & e^{-j\omega_l\frac{N_w-1}{2}T_s} \end{bmatrix} e^{j\omega_l t_r} \quad (3)$$

which is the phase-rotation matrix and

$$\mathbf{A}_l = \mathbf{A}(K_l) = \frac{1}{2}\begin{bmatrix} 1 & \dfrac{N_w-1}{2}T_s & \dfrac{\left(\frac{N_w-1}{2}T_s\right)^2}{2} & \cdots & \dfrac{\left(\frac{N_w-1}{2}T_s\right)^{K_l}}{K_l!} \\ \vdots & \vdots & \vdots & & \vdots \\ 1 & 0 & 0 & & 0 \\ \vdots & \vdots & \vdots & & \vdots \\ 1 & -\dfrac{N_w-1}{2}T_s & \dfrac{\left(-\frac{N_w-1}{2}T_s\right)^2}{2} & \cdots & \dfrac{\left(-\frac{N_w-1}{2}T_s\right)^{K_l}}{K_l!} \end{bmatrix}. \quad (4)$$

According to (1), (3), and (4), the vector of the samples around the measurement instant is approximated through a linear combination between the columns of $\bar{\mathbf{B}}$. The generic expression of the column in the first half of the matrix, corresponding to the kth order term of the lth component, is given by

$$\mathbf{c}_{l,k}[n] = \frac{(nT_s)^k}{2k!} e^{j\omega_l(t_r+nT_s)} \tag{5}$$

with $n = -\frac{N_w-1}{2}, \ldots, \frac{N_w-1}{2}$. Since $x(t)$ is real-valued, for each column vector defined by (5), the second half of $\bar{\mathbf{B}}$ always includes its complex conjugate.

The target is estimating the parameters of the signal model (1), namely, the synchrophasor derivatives that are the entries of $\bar{\mathbf{p}}$. A straightforward yet effective approach is minimizing the mean square error of the mismatch between samples and model output, and therefore,

$$\hat{\bar{\mathbf{p}}}(t_r) = \arg\min_{\bar{\mathbf{p}}} \left\| \bar{\mathbf{B}}\bar{\mathbf{p}} - \mathbf{x}(t_r) \right\| \tag{6}$$

and symbol $\hat{}$ indicates, from here on, estimated quantities.

Assuming full column rank, the solution is provided due to the Moore–Penrose inverse $\bar{\mathbf{B}}^{\dagger}$, thus,

$$\hat{\bar{\mathbf{p}}}(t_r) = \bar{\mathbf{B}}^{\dagger}\mathbf{x}(t_r) = \bar{\mathbf{H}}\mathbf{x}(t_r) \tag{7}$$

where $\bar{\mathbf{H}} = (\bar{\mathbf{B}}^{\mathsf{H}}\bar{\mathbf{B}})^{-1}\bar{\mathbf{B}}^{\mathsf{H}}$ is a bank of complex-valued FIR filters. In particular, the mth row $\bar{\mathbf{H}}_{m,*}$ contains the filter coefficients that permit estimating the mth element of $\hat{\bar{\mathbf{p}}}$, which is the corresponding synchrophasor derivative. Considering the parameters vector defined in (2), assuming that the first component included in the model is the fundamental (i.e., $\bar{X}_1^{(k)}$ is the kth derivative of the fundamental synchrophasor) and assuming that $K_1 \geq 2$, we are mainly interested in estimating the entries $m = 1, 2, 3$, i.e, the fundamental component synchrophasor ($\bar{X}_1^{(0)}$) and its first- and second-order derivatives ($\bar{X}_1^{(1)}$ and $\bar{X}_1^{(2)}$, respectively), which can be employed to obtain frequency and ROCOF estimates ($\widehat{f_1}$ and $\widehat{\text{ROCOF}}$, respectively) [11].

B. Compressive Sensing Solution

Equation (1) defines the class of TFM models: $\mathbf{x}$ is decomposed in the linear combination between the columns of $\bar{\mathbf{B}}$, hence into a set of slowly modulated frequency components. For best performance, it should include the most relevant ones for the estimation process among those present in the observed segment of the signal $x(t)$. Therefore, it should not be defined once and for all, but it might change in every measurement instant, according to the specific operating conditions. Let us suppose that it consists of no more than $Q_{\max}$ components.

As described in [14], its spectral support $\mathcal{S}$ can be built using a predetermined grid of possible angular frequency values with a given step $\delta\omega$ (called super-resolution if $< \frac{2\pi}{N_w T_s}$), while finding the most appropriate candidates through an iterative process, being i the generic iteration index. The TFM approach searches a sparse support made of components belonging to the previously introduced grid, which means looking for the set

$$\mathcal{S} = \left\{ \hat{h}_i, i \in \{1, \ldots, N_{\mathcal{S}}\}, \hat{h}_i = \arg\max_{h\in\Gamma_i} \left| \bar{\mathbf{d}}_h^{\mathsf{H}} \mathbf{r}_{i-1} \right| \right\} \tag{8}$$

where $N_{\mathcal{S}}$ is the cardinality of $\mathcal{S}$ and $\Gamma_i \subseteq \Gamma = \{0, 1, \ldots, N_H\}$ is the set of candidate indexes viable for being added to the support during the ith iteration. Γ is the set of the indexes of the components belonging to the grid, corresponding to the frequency values $\delta\omega$. $\bar{\mathbf{d}}_h$ is the hth column of the dictionary matrix $\bar{\mathbf{D}}$, i.e., the generic atom of the dictionary, and it corresponds to the discrete complex exponential with angular speed $h\delta\omega$, namely, to $\mathbf{c}_{l,0}$ (with l the corresponding component index) when selected in $\mathcal{S}$. Furthermore,

$$\mathbf{r}_i = \mathbf{x} - \bar{\mathbf{B}}_i \hat{\bar{\mathbf{p}}}_i \tag{9}$$

represents the residual after the ith step, where $\bar{\mathbf{B}}_i$ and $\hat{\bar{\mathbf{p}}}_i$ are the matrix defining the model identified at the ith step and the corresponding estimated parameters vector, respectively.[1] Indeed, at the ith iteration, the support found in the previous iteration $\mathcal{S}_{i-1}$ is expanded into $\mathcal{S}_i$ by choosing a new component from the frequency grid, specifically that resulting in the largest projection on $\mathbf{r}_{i-1}$, since it is somewhat expected that it will produce the largest decrease of the residual once it has been included into the model. The model (1) is then adjusted according to the new support $\mathcal{S}_i$, thus defining an augmented model matrix $\bar{\mathbf{B}}_i$ that now includes the new component, its negative frequency image, and their derivatives. Finally, the estimation problem (6) is solved to find $\hat{\bar{\mathbf{p}}}_i$ and the new residual $\mathbf{r}_i$ is computed from (9). The process stops when the cardinality of $\mathcal{S}_i$ reaches $Q_{\max}$ or when the energy of the residual is below a threshold θ_{noise}, which can be defined considering the minimum detection level for spectral components or the expected background noise level.

III. Improved Support Recovery: The CS-EWTFM Approach

A. Weighting and Dictionary Coherence

It is worth highlighting that there is no guarantee that (8) provides the optimal identification of the spectral lines that are actually present in the observed signal according to the super-resolved grid, particularly in the presence of dynamic conditions (that enlarge the component bandwidths) or components having small frequency separation. From a formal point of view, the similarity between the atoms of a given dictionary $\bar{\mathbf{D}}$ (hence the capability to distinguish between them) is quantified by its coherence [24]

$$\mu = \max_{h,k\neq h} \mu_{h,k} \tag{10}$$

where h and k span all the possible combinations among noncoincident column indexes, while

$$\mu_{h,k} = \frac{\left| \bar{\mathbf{d}}_h^{\mathsf{H}} \bar{\mathbf{d}}_k \right|}{\left\| \bar{\mathbf{d}}_h \right\| \left\| \bar{\mathbf{d}}_k \right\|} \tag{11}$$

is the inter-atom coherence, which can be interpreted as a measure of similarity between a pair of dictionary columns.

[1] For $i = 1$, in (8), it is assumed $\mathbf{r}_{i-1} = \mathbf{r}_0 = \mathbf{x}$.

Reminding the expression of $\bar{\mathbf{d}}_h$, (11) can be rewritten as the magnitude of a Dirichlet kernel

$$\mu_{h,k} = \left| \frac{\sin\left(\pi\, \Delta f_{h,k} N_w T_s\right)}{N_w \sin\left(\pi\, \Delta f_{h,k} T_s\right)} \right| \tag{12}$$

where

$$\Delta f_{h,k} = (h-k)\frac{\delta\omega}{2\pi} \tag{13}$$

represents the difference between the frequencies of the atoms indexed by h and k. According to μ, it is possible to define *a priori* the uncertainty of the support recovery stage as a function of the desired sparsity level [25].

By definition, μ is bounded in the range [0, 1], where 0 and 1 correspond, respectively, to a dictionary consisting of mutually orthogonal atoms or to the presence of repeated vectors, differing just by a scale factor. From (12) and (13), μ strongly depends on the selected value of $\delta\omega$. In our case, TFM relies on a super-resolved frequency grid, which implies that $\mu < 1$. On the one hand, a finer frequency resolution potentially enables a better match between signal and model, which translates into higher performance and disturbance rejection. On the other hand, coherence degrades as $\delta\omega$ is reduced, and thus, there is higher chance to select the wrong signal support. Therefore, selecting the frequency grid comes out as the result of a tradeoff between these opposite requirements.

In order to improve accuracy, we want to investigate whether, for the same grid step $\delta\omega$, it is possible to transform the dictionary in order to decrease the coherence between the most critical atoms. In this respect, we can consider using weighting windows, widely employed in frequency-domain analysis [26], [27]. When the target is extracting a spectral component, we could dramatically reduce the spectral interference with respect to the others present in the signal, due to the lower sidelobes in the frequency-domain content of the window. Therefore, we want to scout if properly applying weighting to the atoms in the dictionary $\bar{\mathbf{D}}$ has a beneficial impact on coherence.

Let us introduce $\mathbf{w} = \left[w_1 \cdots w_{N_w}\right]^\intercal$ as the real-valued vector of the weights. We define a new dictionary matrix $\bar{\mathbf{G}}$ whose generic column is

$$\bar{\mathbf{g}}_h = \mathbf{w} \circ \bar{\mathbf{d}}_h \tag{14}$$

where $\circ$ denotes the Hadamard product. Using (11), we obtain the expression of the coherence between atoms in the weighted dictionary, which is

$$\mu_{h,k} = \frac{\left| \sum_{n=-\frac{N_w-1}{2}}^{\frac{N_w-1}{2}} w^2_{n+\frac{N_w+1}{2}} e^{-j2\pi\, \Delta f_{h,k} n T_s} \right|}{\|\mathbf{w}\|^2}. \tag{15}$$

It is extremely significant to observe that $\mu_{h,k}$ represents the normalized magnitude of the DTFT of the vector of the squared weights (therefore an even function) evaluated in $\Delta f_{h,k}$. Hence, if the weights correspond to the square root of a window function, the coherence reflects its spectral content. The target is thus choosing the window function that enables better support recovery under the operating conditions that PMUs may face. To fix the ideas, let us consider a sampling rate $f_s = 5$ kHz and $N_w = 431$. In this context, Fig. 1 reports $\mu_{h,k}$ between the columns of $\bar{\mathbf{G}}$ as a function of the absolute value of $\Delta f_{h,k}$.

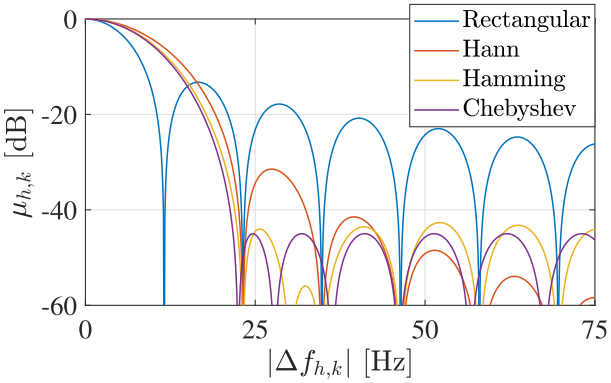

Fig. 1. Coherence as a function of the frequency separation between atoms for different weighting windows.

It is not surprising that, when the rectangular window is adopted (therefore $\bar{\mathbf{G}} = \bar{\mathbf{D}}$), the coherence plot exhibits the narrowest main lobe, namely, the lowest similarity between atoms having small frequency separation (below 14 Hz). However, the slowly decaying sidelobes make $\mu_{h,k}$ remain significant even in case of fairly large values of $\Delta f_{h,k}$: this may lead to errors during support recovery because of cumulative leakage effects. In particular, the third lobe brings coherence above 0.12 around 30 Hz: considering reporting rates of 50 fps and above, this could undermine the detection and suppression of OoB interference, which notably represents a challenging scenario for PMU algorithms.

When weights are derived from a Hann window, $\mu_{h,k}$ shows the main lobe having double width when compared to the previous case, but, as expected, the sidelobes quickly decrease. This is a significant benefit with respect to the rectangular window, but the coherence in the critical region for OoB interference rejection remains still significant because of the first sidelobe.

The most natural choice to overcome this limitation is choosing the Hamming window, namely, the two-term cosine window aimed at minimizing the height of the first sidelobe. As shown in Fig. 1, we have the additional benefit of smaller coherence between nearby atoms. However, even better results can be reached if weights are obtained from a Chebyshev window having 45 dB sidelobe magnitude attenuation. It is worth noticing how the obtained coherence resembles the pass bandwidth of a PMU with a reporting rate of 50 fps. The main lobe becomes slightly narrower and, more important, the maximum magnitude of the sidelobes is further reduced; thus, better detection of frequency components is expected.

B. Enhanced Support Recovery

In order to exploit the potential benefits of dictionary $\bar{\mathbf{G}}$, the TFM approach must be properly modified, thus leading to the weighted TFM (CS-WTFM or WTFM in the following) approach. Let us start from the TFM model (1) and let us multiply both the members by matrix diag($\mathbf{w}$), whose diagonal

entries are the elements of $\mathbf{w}$, thus obtaining

$$\mathbf{w} \circ \mathbf{x}(t_r) = \text{diag}(\mathbf{w})\bar{\mathbf{B}}\bar{\mathbf{p}}(t_r) + \mathbf{r}^w = \bar{\mathbf{B}}^w\bar{\mathbf{p}}(t_r) + \mathbf{r}^w \quad (16)$$

where $\mathbf{r}^w$ is the weighted version of the mismatch between model and samples. Reminding (3), (4), and (14), $\bar{\mathbf{B}}^w$ can be obtained as the solution of the CS problem using dictionary $\bar{\mathbf{G}}$ instead of $\bar{\mathbf{D}}$. The weighted samples can be used to look for $\mathcal{S}^w$ through a modified procedure. The support set $\mathcal{S}^w$ is redefined as

$$\mathcal{S}^w = \left\{\hat{h}_i,\ i \in \{1, \ldots, N_{\mathcal{S}^w}\},\ \hat{h}_i = \arg\max_{h \in \Gamma_i^w} \left|\bar{\mathbf{g}}_h^{\mathsf{H}}\mathbf{r}_{i-1}^w\right|\right\} \quad (17)$$

where $\mathbf{r}_{i-1}^w$ is the residual of the weighted samples before the ith iteration, $N_{\mathcal{S}^w}$ is the cardinality of $\mathcal{S}^w$, and Γ_i^w represents the set of candidate indexes to be added to the support at the ith step. The step-by-step procedure resembles that of the TFM approach for synchrophasor, frequency, and ROCOF estimation, and it just requires weighting the samples while using the weighted dictionary. Estimated signal parameters at the ith iteration read as

$$\hat{\bar{\mathbf{p}}}_i^w = \arg\min_{\bar{\mathbf{p}}} \left\|\mathbf{w} \circ \mathbf{x} - \bar{\mathbf{B}}_i^w\bar{\mathbf{p}}\right\|. \quad (18)$$

It is also interesting to notice that

$$\bar{\mathbf{g}}_h^{\mathsf{H}}\mathbf{r}_{i-1}^w = \left(\mathbf{w} \circ \bar{\mathbf{d}}_h\right)^{\mathsf{H}}\mathbf{r}_{i-1}^w = \bar{\mathbf{d}}_h^{\mathsf{H}}\left(\mathbf{w} \circ \mathbf{r}_{i-1}^w\right). \quad (19)$$

For $i = 1$, (19) corresponds to ($^\circ$ indicates the Hadamard power)

$$\bar{\mathbf{g}}_h^{\mathsf{H}}\mathbf{r}_0^w = \bar{\mathbf{d}}_h^{\mathsf{H}}\left(\mathbf{w}^{\circ 2} \circ \mathbf{x}\right) \quad (20)$$

and thus, it is equivalent to adopt the original dictionary $\bar{\mathbf{D}}$ but weighting the samples with the square of $\mathbf{w}$.

Although the introduction of weighting significantly improves support recovery, as discussed in [22], it does not guarantee that the solution of the CS problem leads to the optimal signal model, in particular in the presence of interharmonic disturbances. In this article, we propose a simple technique to refine support recovery, thus leading to more accurate measurements. The idea is exploiting the estimated signal model in order to detect whether it is consistent with the selected support. Specifically, let us assume that we are in the generic ith iterative step; we have just added the component $\hat{h}_i$ to the support, thus obtaining $\mathcal{S}_i^w$. Considering the generic lth component included in the support, supposing that it has position $h(l)$ on the super-resolved frequency grid, let us assume that $K_l \geq 1$, namely that at least a first-order expansion has been included into the model. The values and the derivatives of the components included in the support can be obtained through (18). Furthermore, for each l, we can evaluate the corresponding angular frequency deviation with respect to $h(l)\delta\omega$ as

$$\widehat{\Delta\omega}(l) = \frac{\Im\left[\hat{\bar{X}}_l^{(1)} \cdot \underline{\hat{X}}_l^{(0)}\right]}{\left|\hat{\bar{X}}_l^{(0)}\right|^2} \quad (21)$$

where $\Im[\cdot]$ is the imaginary part operator.

The magnitude of this angular frequency deviation should be lower than half of the super-resolution step $\delta\omega$ if the support has been properly retrieved. If this condition is not verified, there is high probability that the lth atom in the support is not the best approximation for the component actually present in the observed signal. Therefore, a better signal model is obtained if the lth component in the support is replaced with that whose position on the grid is

$$\hat{h}^{\text{ref}}(l) = h(l) + \text{round}\left(\frac{\widehat{\Delta\omega}(l)}{\delta\omega}\right). \quad (22)$$

Once this procedure has been carried out for all the components present in $\mathcal{S}_i^w$, if at least one of them has been moved, the corresponding matrix $\bar{\mathbf{B}}_i^{w,\text{ref}}$ of the refined model is obtained. A better estimate $\hat{\bar{\mathbf{p}}}_i^{w,\text{ref}}$ of the signal parameters is derived from (18) using the new matrix $\bar{\mathbf{B}}_i^{w,\text{ref}}$. Frequency and ROCOF are finally computed by means of the formulas reported in [11]. The steps of the proposed approach (EWTFM in the following) are summarized by Algorithm 1.

Algorithm 1: CS-EWTFM

Input: $\mathbf{x}$, $\bar{\mathbf{G}}$, $\mathbf{w}$, θ_{noise}
Output: $\mathcal{S}^w$, $\hat{\bar{\mathbf{p}}}^{w,\text{ref}}$
initialize $i = 1$, $\mathcal{S}_0^w = \emptyset$, $\bar{\mathbf{B}}_0^w = \emptyset$, $\bar{\mathbf{B}}_{0,\frac{1}{2}}^w = \emptyset$
initialize residual $\mathbf{r}_0^w = \mathbf{w} \circ \mathbf{x}$
compute residual energy $\text{E}_{\text{res}} = \|\mathbf{r}_0^w\|^2$
while $\text{E}_{\text{res}} \geq \theta_{\text{noise}}$ & $i \leq Q_{\max}$ **do** - *support search*
  consider an appropriate Γ_i^w depending on the needs
  find the index $\hat{h}_i = \arg\max_{h \in \Gamma_i^w} |\bar{\mathbf{g}}_h^{\mathsf{H}}\mathbf{r}_{i-1}^w|$
  update $\mathcal{S}_i^w = \mathcal{S}_{i-1}^w \cup \{\hat{h}_i\}$
  define $\mathbf{A}(K_i)$ with K_i order of expansion of the new component
  update $\bar{\mathbf{B}}_{i,\frac{1}{2}}^w = [\bar{\mathbf{B}}_{i-1,\frac{1}{2}}^w \quad \text{diag}(\mathbf{w})\Phi(\hat{h}_i\delta\omega)\mathbf{A}(K_i)]$
  update $\bar{\mathbf{B}}_i^w = [\bar{\mathbf{B}}_{i,\frac{1}{2}}^w \quad \underline{\bar{\mathbf{B}}}_{i,\frac{1}{2}}^w]$
  find $\hat{\bar{\mathbf{p}}}_i^w = \arg\min_{\bar{\mathbf{p}}} \|\mathbf{w} \circ \mathbf{x} - \bar{\mathbf{B}}_i^w\bar{\mathbf{p}}\|$
  compute $\hat{h}^{\text{ref}}(l) \quad \forall l \in \{1, \ldots, i\}$ using (22)
  if $\exists\, l \mid \hat{h}^{\text{ref}}(l) \neq h(l)$ **then** - *support refinement*
    update $\mathcal{S}_i^w$ and define $\bar{\mathbf{B}}_i^{w,\text{ref}}$ accordingly
    find $\hat{\bar{\mathbf{p}}}_i^{w,\text{ref}} = \arg\min_{\bar{\mathbf{p}}} \|\mathbf{w} \circ \mathbf{x} - \bar{\mathbf{B}}_i^{w,\text{ref}}\bar{\mathbf{p}}\|$
  end
  update $\mathbf{r}_{i+1}^w = \mathbf{w} \circ \mathbf{x} - \bar{\mathbf{B}}_i^w\hat{\bar{\mathbf{p}}}_i^{w,\text{ref}}$
  update $\text{E}_{\text{res}} = \|\mathbf{r}_{i+1}^w\|^2$
  update $i = i + 1$
end
return

IV. Tests and Results

The performance of the proposed approach has been assessed through numerical simulations. A comparison is also given with the TFM approach proposed in [14] and the WTFM approach presented in [22]. The sampling rate is $f_s = 5$ kHz, namely, the same adopted in Section III-A. Frequency resolution $\delta\omega$ is a key parameter, which, as previously discussed, comes out as a tradeoff between the flexibility of the TFM model (thus setting the theoretical accuracy bound) and the probability of retrieving the optimal frequency support; in this respect, $\delta\omega = 1$ Hz is selected. For all the algorithms, the

expansion order for the truncated Taylor series is $K_1 = 2$ for the fundamental and $K_l = 1$ for all the other components. Accuracy in synchrophasor, frequency, and ROCOF estimations has been quantified in terms of TVE, FE, and RFE under challenging static and dynamic conditions, which have been specifically designed to stress the algorithms. The three adopted indexes are given by the following expressions:

$$\begin{aligned} \text{TVE} &= \frac{\left|\hat{\bar{X}}_1^{(0)} - \bar{X}_1^{(0)}\right|}{\left|\bar{X}_1^{(0)}\right|} \\ \text{FE} &= \widehat{f_1} - f_1 \\ \text{RFE} &= \widehat{\text{ROCOF}} - \text{ROCOF}. \end{aligned} \tag{23}$$

In the following, the performed tests are divided into steady-state and dynamic conditions and are used to highlight the differences among the algorithms with a given underlying model. $N_w = 431$ samples are used for each window and the weighting vector $\mathbf{w}$ of both WTFM and EWTFM is given by the square root of Chebyshev window, as described in Section III-A. Then, additional tests intended to analyze the impact of the configuration on the proposed approach are described. All the test waveforms used in the following are defined by modifying the parameters of a base signal. It features a fundamental frequency of 50.55 Hz, i.e., it does not coincide with the nominal system rate and it does not belong to the super-resolved frequency grid. Moreover, the signal support consists also of an interharmonic component (10% at 19.7 Hz) and the second and third harmonics (2% and 5%, respectively). In this way, the leakage contributions are maximized and the algorithms are tested in a nearly worst case scenario.

A. Steady-State Tests

The test duration has been set equal to 10 s and a reporting rate of 100 fps is considered.

The first test is derived from the signal frequency range of the IEC Std off-nominal frequency tests and the fundamental frequency f varies from 45 to 55 Hz with 0.1-Hz step. The frequency set is arranged so that the base frequency of 50.55 Hz is included.

Fig. 2(a)–(c) shows the estimation results in terms of maximum TVE, |FE|, and |RFE|, respectively. The errors depend on the fundamental frequency since they are affected by the impact of long-term leakage of disturbances and, in particular, of the interharmonic component. Table I reports the maximum errors in the worst case condition (labeled as off-nominal). As expected from the results in [22], the approaches based on windowing clearly outperform the TFM, but EWTFM presents lower and much flatter errors with respect to WTFM too. Indeed, the error reduction is up to about 80% for several frequencies and all the error indexes. This performance is mostly due to a better frequency support recovery, mainly concerning the interharmonic location. When comparing EWTFM with WTFM, the most significant improvements occur for frequency and ROCOF estimates, while TVE values are already very small, in particular if we compare them with the typical accuracy of instrument transformers.

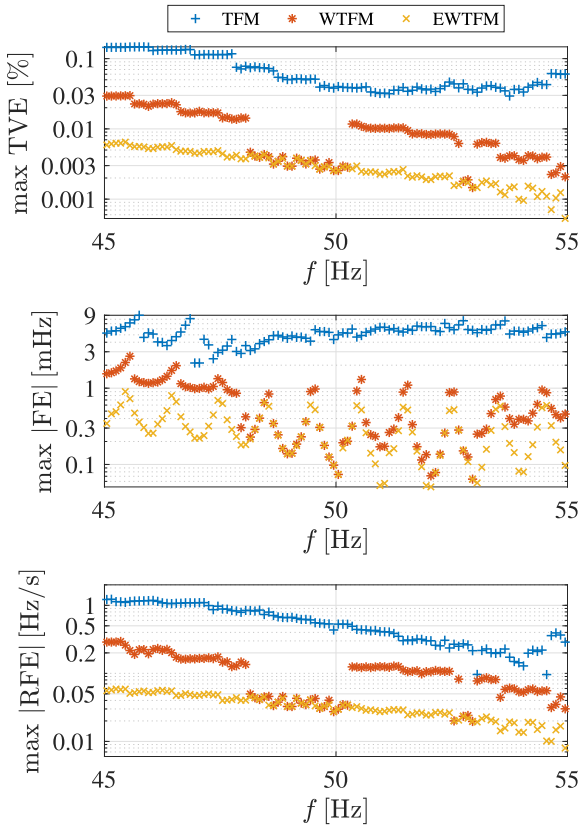

Fig. 2. Maximum errors as a function of the fundamental frequency for TFM (plus sign), WTFM (asterisk), and EWTFM (cross).

The maximum estimation errors of EWTFM are well below 0.01%, 0.1 mHz, and 0.1 Hz for synchrophasor (considering vector error), frequency, and ROCOF measurements, respectively, which represents a remarkable result in the presence of such challenging input signals.

To assess also the robustness in the presence of wideband noise, tests have been performed by adding a white uniform noise to the samples of the base signal at different levels of signal-to-noise ratio (SNR). Table II reports a selection of the obtained maximum TVE, |FE| and |RFE| values. The results confirm that windowing improves the performance. Also, under this condition, EWTFM provides a better retrieval of the signal components and thus allows higher estimation accuracy. For instance, with SNR= 75 dB, the maximum |FE| goes from 1.36 mHz with WTFM to 0.75 mHz (almost halved) with EWTFM. The error reduction brought by EWTFM is more pronounced at higher SNRs, while it is less significant at 60 dB (about 6% for RFE and negligible for TVE and FE). It is interesting to highlight that noise influences accuracy through two different effects: it affects support recovery, and it is transferred from the samples to the estimates according to the effective noise bandwidth of the adopted window. The former one is predominant since WTFM and EWTFM adopt the same window.

Table I also reports (second column) the maximum errors corresponding to the worst case scenario when the OoB interference frequency is varied. During the OoB tests, the

TABLE I

WORST CASE PERFORMANCE COMPARISON IN STEADY-STATE CONDITIONS

Index	Algorithm	Off-nominal	Out-of-Band
TVE [%]	TFM	0.147	0.254
	WTFM	0.030	0.095
	EWTFM	0.006	0.011
FE [mHz]	TFM	9.03	13.26
	WTFM	2.62	4.64
	EWTFM	0.90	1.27
RFE [Hz/s]	TFM	1.23	1.86
	WTFM	0.29	1.28
	EWTFM	0.06	0.09

TABLE II

PERFORMANCE COMPARISON IN THE PRESENCE OF WIDEBAND NOISE

Index	Algorithm	SNR [dB]						
		60	65	70	75	80	85	90
TVE [%]	TFM	0.066	0.049	0.041	0.041	0.040	0.039	0.039
	WTFM	0.037	0.022	0.016	0.013	0.012	0.011	0.011
	EWTFM	0.037	0.022	0.014	0.008	0.005	0.004	0.003
FE [mHz]	TFM	5.64	5.09	5.00	4.99	4.91	4.91	4.91
	WTFM	2.09	1.67	1.36	1.36	1.32	1.32	1.30
	EWTFM	2.09	1.27	1.03	0.75	0.63	0.57	0.56
RFE [Hz/s]	TFM	0.54	0.47	0.46	0.45	0.44	0.44	0.44
	WTFM	0.19	0.13	0.13	0.12	0.12	0.12	0.12
	EWTFM	0.18	0.09	0.07	0.05	0.04	0.03	0.03

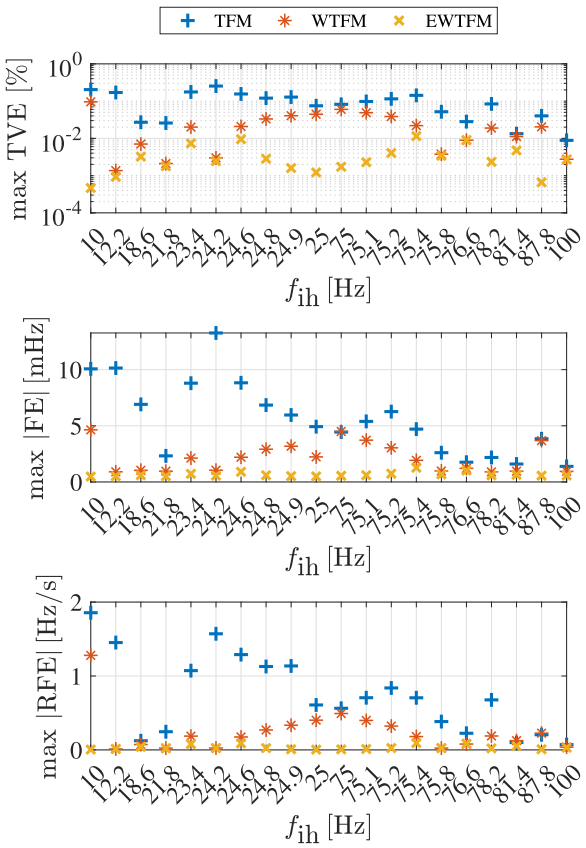

Fig. 3. Maximum errors as function of the interharmonic frequency for TFM (plus sign), WTFM (asterisk), and EWTFM (cross).

fundamental frequency is kept at 50.55 Hz, and the second- and third-order harmonic components are present, whereas the interharmonic frequency f_{ih} varies within the bandwidth provided by the IEC Std for 50-fps reporting rate, namely, from 10 to 25 Hz (OoB subharmonics) and from 75 to 100 Hz. In compliance with the IEC Std test specifications, both the intervals have been spanned by selecting ten test points distributed with a logarithmic scale.

Fig. 3 shows the maximum values of the error indexes as a function of the interharmonic frequency. The WTFM improves significantly the estimation accuracy with respect to TFM apart from the boundaries of the PMU pass bandwidth, i.e., at 25 and 75 Hz and at $f_{ih} = 10$ Hz, where the proximity to the image component makes it extremely challenging to retrieve the optimal support. The EWTFM provides an accurate support recovery regardless of the considered interharmonic frequency in the whole OoB range, leading to remarkable estimation errors. The advantage is more evident precisely where WTFM suffers from close interharmonic interference, as shown, for instance, by RFE results for the test frequencies between 24.6 and 75.4 Hz. The results in Table I highlight that, in the worst case, TVE and RFE values for EWTFM are reduced by about one order of magnitude with respect to WTFM, while FE decreases by about 73% (i.e., one order of magnitude less than TFM). When $f_{ih} = 10$ Hz, that is, the worst case of TFM and WTFM for ROCOF measurements (maximum RFEs are larger than 1 Hz/s), the RFE achieved by EWTFM is less than 0.005 Hz/s.

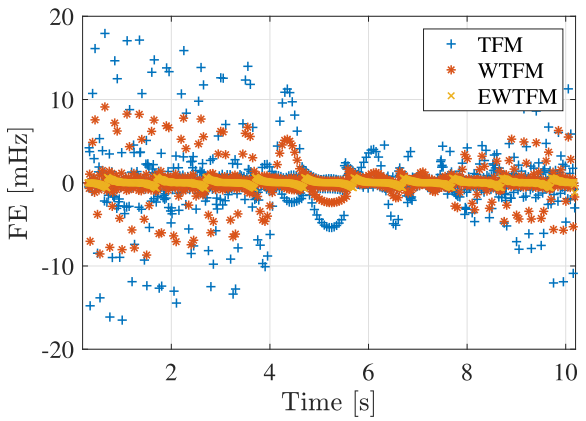

Fig. 4. FE during ramp test for TFM (plus sign), WTFM (asterisk), and EWTFM (cross).

B. Dynamic Tests

After steady-state conditions, the capability to track dynamic variations has been tested. First, the fundamental frequency of the base test signal is changed with time according to a linear ramp (ROCOF $= +1$ Hz/s) in the interval 45–55 Hz. The fundamental frequency spans the whole frequency range used in the off-nominal test, and thus, the interharmonic frequency is set to 10 Hz to better explore the algorithm's performance and check one of the most critical conditions considered in Fig. 3. Fig. 4 shows the evolution

TABLE III
MAXIMUM ERROR INDEXES DURING LINEAR FREQUENCY RAMP TEST

Index	Algorithm		
	TFM	WTFM	EWTFM
TVE [%]	0.207	0.096	0.005
FE [mHz]	17.94	9.10	1.20
RFE [Hz/s]	1.90	1.29	0.12

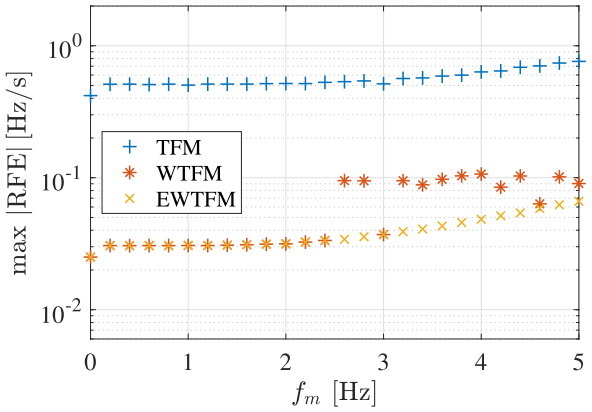

Fig. 5. Maximum |RFE| as a function of the AM frequency for TFM (plus sign), WTFM (asterisk), and EWTFM (cross).

of FE with time during the ramp duration (the ramp lasts for 10 s and the 3.5 cycles after the start and before the end of the ramp have been excluded according to IEC Std). For TFM and WTFM, |FE| decreases as the fundamental component moves far away from the interharmonic and as the frequency approaches the nominal one. The behavior of EWTFM is different and its benefits are evident. FE is almost flat notwithstanding the changing distance between the component of interest and the interharmonic disturbance due to an accurate support recovery. Small jumps in the error, corresponding to a support change in the super-resolved grid, are also visible, thus reflecting the tracking capability. Maximum |FE| (see Table III) decreases from 17.94 mHz of TFM to 1.20 mHz of EWTFM, thus showing that the latter achieves an error reduction of about one order of magnitude with respect to the other algorithms. Similar general considerations, even if with different time patterns, can be drawn for TVE and RFE, whose maximum values are reported in Table III, confirming the error reduction for all the indexes.

Sinusoidal amplitude modulation (AM) and phase modulation (PM) of the fundamental component have been included in the test waveforms, always in the presence of the harmonic and interharmonic disturbances of the base waveform. The fundamental frequency is kept at 50 Hz, while the modulation frequency f_m is varied from 0 to 5 Hz (as in the M-class compliance tests [5]) with 0.2-Hz step. The AM modulation depth is set to 0.1 p.u., while the PM amplitude is 0.1 rad, according to the IEC Std.

Fig. 5 shows the maximum |RFE| during the AM test as a function of f_m. WTFM largely improves the ROCOF estimation with respect to TFM, as already proven in [22], but EWTFM brings an additional error reduction at higher modulation frequencies (e.g., when $f_m = 2.6$ Hz, |RFE| is 0.10 and 0.03 Hz/s for WTFM and EWTFM, respectively). The similarities and differences between WTFM and EWTFM can be explained as follows. At low modulation frequencies ($f_m \leq 2.4$ Hz), there are no support recovery errors for WTFM since the fundamental component has the nominal frequency and is thus always located on the super-resolved grid. In addition, the bandwidth of the time-varying component associated with fundamental frequency is narrow. EWTFM and WTFM thus provide the same measurements since the same frequency support is found. When the bandwidth of the fundamental component starts widening at higher modulation frequencies, more interactions with the disturbances occur, and thus, the support recovery of WTFM is less effective, while EWTFM is able to refine it, leading to better estimation results. This improvement is particularly evident in terms of ROCOF estimation since it is notably the most affected by interference from harmonic and interharmonic components, thus by errors in support recovery. Similar considerations hold also for TVE and FE, but, for the aforementioned reason, the differences between the two approaches are negligible in this case.

During PM test conditions, the fundamental frequency deviates from its nominal value proportionally to f_m, up to a maximum of 0.5 Hz. Again, we are always close to the nominal rate and the reference point on the super-resolved grid is always the same. As in case of AM, at low modulation frequencies (below 2.6 Hz), WTFM and EWTFM are the same and lead to much more accurate synchrophasor, frequency, and ROCOF measurements than TFM; errors are more than halved (see [22] for RFE). At higher frequencies, differences between WTFM and EWTFM emerge, but they are often masked when looking at maximum errors since support retrieval errors of WTFM are few and they do not correspond to maximum error conditions because of the complex interactions of leakage effects. Anyway, WTFM and EWTFM approaches' errors are much lower than TFM (at least -49%, -28%, and -25% for TVE, FE, and RFE, respectively), but they are very close and are not reported here for the sake of brevity.

One of the reasons for this similarity between the performance of WTFM and EWTFM under modulations can be the error floor given by the model mismatch. Indeed, when frequency ramp is considered, the constant ROCOF guarantees that the second-order model is fit for modeling the component of interest, but with PMs, for instance, this is no longer true. Then, modulation tests have been repeated in the same conditions, changing only the expansion order K_1 of the fundamental component to 3. Among the new results, Fig. 6 shows the maximum |FE| as a function of the modulation frequency for PM. Error values are much lower than those obtained with $K_1 = 2$, which are up to 82.97, 59.87, and 59.68 mHz for TFM, WTFM, and EWTFM, respectively, when $f_m = 5$ Hz. Furthermore, EWTFM helps further reduce the FE beyond WTFM results. We can notice that the distance between the two curves is between 2.38 and 2.98 mHz and remains nearly constant with the modulation frequency, leading to improvements between 37% and 79%. Similar trends can also be observed for TVE and |RFE|

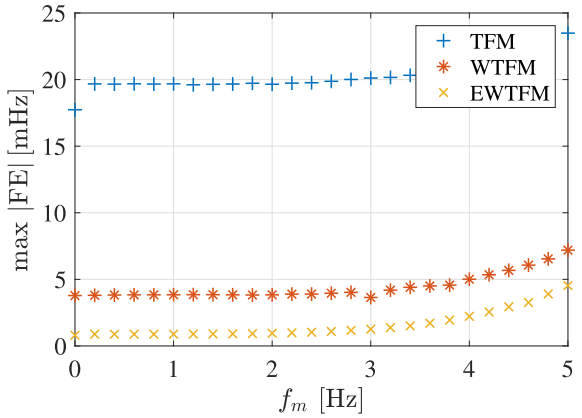

Fig. 6. Maximum |FE| as a function of the phase-angle modulation frequency for TFM (plus sign), WTFM (asterisk), and EWTFM (cross) when $K_1 = 3$.

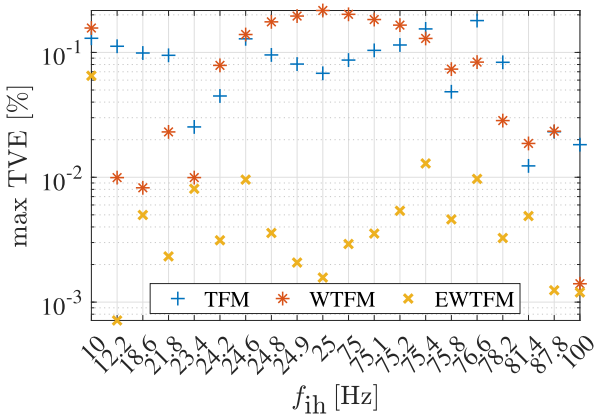

Fig. 7. Maximum TVE as a function of the interharmonic frequency for TFM (plus sign), WTFM (asterisk), and EWTFM (cross) when $N_w = 399$.

plots, and thus, they are not reported for the sake of brevity. In conclusion, the EWTFM is always more effective than the other algorithms also in the presence of modulations.

Since the performance of EWTFM is always better than that of TFM and WTFM and helps push the errors far below standard limits, we have verified also the sensitivity of the algorithm when the window length is reduced. In particular, we have assessed the performance when $N_w = 399$, i.e., less than four nominal cycles, which constitutes a limit for the P-class algorithm in IEC Std and thus represents an interesting turning point. Fig. 7 shows a relevant example of the obtained results. The maximum TVE is reported for the OoB test, carried out as described above. When compared to Fig. 3 (top figure), WTFM is affected by the reduced selectivity due to a shorter window length and its performance is worse than that of TFM particularly when the interharmonic component is closer to the fundamental one. EWTFM, thanks to its enhanced support retrieval, is still the most accurate algorithm (e.g., maximum TVE -98% and -95% with respect to TFM and WTFM, respectively, for $f_{\text{ih}} = 75$ Hz).

EWTFM is designed to suitably compensate for spurious interferences in dynamic conditions. In order to validate this feature, we have compared its performance against the iterative interpolated DFT (iIpDFT). As shown in [28], the iIpDFT is a synchrophasor estimation algorithm that relies on a static signal model, but it adaptively rejects the injections from harmonic and interharmonic components and proves, when properly configured, to be compliant with both P- and M-class requirements of the IEC Std. For this analysis, we considered two of the previous test conditions: the steady-state test with fundamental frequency equal to 50.55 Hz and the AM test with modulation frequency equal to 2 and 5 Hz. For the sake of comparability, the iIpDFT has been configured with a Hann window, whose duration is four nominal cycles. Given a reporting rate of 50 fps, each test has 3-s duration and the worst case performance indexes are reported in Table IV.

TABLE IV
PERFORMANCE COMPARISON EWTFM VERSUS IIPDFT

Index	Algorithm	Test steady -state	Test AM $f_m = 2$ Hz	Test AM $f_m = 5$ Hz
TVE [%]	EWTFM	0.003	0.005	0.062
	iIpDFT	0.017	0.820	2.303
FE [mHz]	EWTFM	0.51	0.18	0.54
	iIpDFT	0.68	29.10	83.82
RFE [Hz/s]	EWTFM	0.04	0.06	0.18
	iIpDFT	0.01	2.43	5.74

The error comparison confirms the remarkable performance of the iIpDFT algorithm in steady-state conditions, whereas the dynamic tests show a significant accuracy degradation, proportional to the modulation frequency. Conversely, the EWTFM guarantees a nearly constant performance in all the tests. The motivation has to be found in two aspects. First, the EWTFM relies on a dynamic signal model that better fits a signal with AM. Second, the iIpDFT approach has more difficulty in identifying the interharmonic component due to the larger leakage coming from the fundamental component.

C. Considerations on Computation Time

EWTFM involves a frequency support refinement step, which leads to a further matrix inversion and estimation if the support is updated. The additional computational burden corresponds to the execution of (18) with the new matrix $\bar{\mathbf{B}}_i^{w,\text{ref}}$ to find $\hat{\mathbf{p}}_i^{w,\text{ref}}$. The overall computation time is indeed composed of the support recovery time, the first estimation time, the support refinement time, and the second estimation time. This means that EWTFM almost doubles the estimation time contribution with respect to WTFM (support refinement time is almost negligible), but support recovery time is typically predominant, and thus, the relative increase in computation time is marginal. In addition, the enhanced recovery of the relevant components performed at each iteration by EWTFM might also, under some circumstances, reduce the support cardinality preventing the algorithm from finding spurious components and thus better matching the samples. In this case, the overall computation time might even be reduced.

Tests have been performed to find the average execution time on 500 estimations using a Windows 10 personal computer equipped with Intel Core i7-10510U CPU 1.80 GHz and

16-GB RAM. In particular, assuming that $N_w = 399$ while considering the same test scenario as in Table II (off-nominal frequency, harmonics, interharmonic, and noise), the average estimation time for EWTFM is 2.8 ms with a standard deviation of 0.5 ms. The average increase in computation time with respect to WTFM is about 10%, thus confirming that the most time-consuming step is support recovery. However, it is important to highlight that the adopted code is run in MATLAB and also not optimized. Here, the intent is mainly to show that a real-time computation at a reporting rate of 100 fps can be obtained without particular effort as shown in [15]. The iIpDFT algorithm configured as in Section IV-B and executed under the same test conditions gives an average computation time of 2.8 ms with a standard deviation of 0.4 ms, thus comparable with the proposed approach.

V. Conclusion

This article proposes EWTFM as an enhanced Taylor–Fourier multifrequency model for the estimation of synchrophasor, frequency, and ROCOF. The proposed approach relies on the joint application of a weighting function for minimizing the leakage injections due to spurious components and an iterative spectral support correction based on the estimated first derivative of each component. In particular, the window function improves the dictionary coherence and enables a more precise identification of close-by spectral components, while the derivative correction allows for guaranteeing the best dictionary representation in dynamic conditions and better tracking of time-varying trends. The obtained results highlight the remarkable accuracy improvement that can be reached due to the EWTFM approach under very demanding static and dynamic scenarios. A sensitivity analysis investigates the impact of window length and expansion order on the final estimation accuracy. A thorough performance characterization confirms the potential of the proposed approach that guarantees a remarkable RFE lower than 200 mHz/s even in the presence of concurrent frequency ramps or modulations and high distortion levels.

References

[1] R. Langella, A. Testa, J. Meyer, F. Möller, R. Stiegler, and S. Z. Djokic, "Experimental-based evaluation of PV inverter harmonic and interharmonic distortion due to different operating conditions," *IEEE Trans. Instrum. Meas.*, vol. 65, no. 10, pp. 2221–2233, Oct. 2016.

[2] M. Paolone *et al.*, "Fundamentals of power systems modelling in the presence of converter-interfaced generation," *Electr. Power Syst. Res.*, vol. 189, Dec. 2020, Art. no. 106811.

[3] J. Fang, H. Li, Y. Tang, and F. Blaabjerg, "On the inertia of future more-electronics power systems," *IEEE J. Emerg. Sel. Topics Power Electron.*, vol. 7, no. 4, pp. 2130–2146, Dec. 2019.

[4] J. De La Ree, V. Centeno, J. S. Thorp, and A. G. Phadke, "Synchronized phasor measurement applications in power systems," *IEEE Trans. Smart Grid*, vol. 1, no. 1, pp. 20–27, Jun. 2010.

[5] *IEEE/IEC International Standard—Measuring Relays and Protection Equipment—Part 118-1: Synchrophasor for Power Systems—Measurements*, Standard 60255-118-1:2018, 2018, pp. 1–78.

[6] S. Vejdan, M. Sanaye-Pasand, and O. P. Malik, "Accurate dynamic phasor estimation based on the signal model under off-nominal frequency and oscillations," *IEEE Trans. Smart Grid*, vol. 8, no. 2, pp. 708–719, Mar. 2017.

[7] D. M. Laverty, H. Kirkham, D. J. Morrow, and X. Liu, "Estimation of goodness of fit of synchrophasors during transient faults," in *Proc. IEEE Power Energy Soc. Gen. Meeting*, Jul. 2017, pp. 1–5.

[8] P. S. Wright, P. N. Davis, K. Johnstone, G. Rietveld, and A. J. Roscoe, "Field testing of ROCOF algorithms in multiple locations on Bornholm Island," in *Proc. Conf. Precis. Electromagn. Meas. (CPEM)*, Jul. 2018, pp. 1–2.

[9] I. Kamwa, A. K. Pradhan, and G. Joos, "Adaptive phasor and frequency-tracking schemes for wide-area protection and control," *IEEE Trans. Power Del.*, vol. 26, no. 2, pp. 744–753, Apr. 2011.

[10] G. Rietveld, P. S. Wright, and A. J. Roscoe, "Reliable rate-of-change-of-frequency measurements: Use cases and test conditions," *IEEE Trans. Instrum. Meas.*, vol. 69, no. 9, pp. 6657–6666, Sep. 2020.

[11] J. A. O. De La Serna, "Dynamic phasor estimates for power system oscillations," *IEEE Trans. Instrum. Meas.*, vol. 56, no. 5, pp. 1648–1657, Oct. 2007.

[12] D. Belega, D. Fontanelli, and D. Petri, "Low-complexity least-squares dynamic synchrophasor estimation based on the discrete Fourier transform," *IEEE Trans. Instrum. Meas.*, vol. 64, no. 12, pp. 3284–3296, Dec. 2015.

[13] P. Castello, J. Liu, C. Muscas, P. A. Pegoraro, F. Ponci, and A. Monti, "A fast and accurate PMU algorithm for P+M class measurement of synchrophasor and frequency," *IEEE Trans. Instrum. Meas.*, vol. 63, no. 12, pp. 2837–2845, Dec. 2014.

[14] M. Bertocco, G. Frigo, C. Narduzzi, C. Muscas, and P. A. Pegoraro, "Compressive sensing of a Taylor-Fourier multifrequency model for synchrophasor estimation," *IEEE Trans. Instrum. Meas.*, vol. 64, no. 12, pp. 3274–3283, Dec. 2015.

[15] G. Frigo, A. Derviskadic, Y. Zuo, A. Bach, and M. Paolone, "Taylor-Fourier PMU on a real-time simulator: Design, implementation and characterization," in *Proc. IEEE Milan PowerTech*, Jun. 2019, pp. 1–6.

[16] M. Bertocco, G. Frigo, C. Narduzzi, and F. Tramarin, "Resolution enhancement by compressive sensing in power quality and phasor measurement," *IEEE Trans. Instrum. Meas.*, vol. 63, no. 10, pp. 2358–2367, Oct. 2014.

[17] G. Frigo, P. A. Pegoraro, and S. Toscani, "Low-latency, three-phase PMU algorithms: Review and performance comparison," *Appl. Sci.*, vol. 11, no. 5, p. 2261, Mar. 2021. [Online]. Available: https://www.mdpi.com/2076-3417/11/5/2261

[18] C. Narduzzi, M. Bertocco, G. Frigo, and G. Giorgi, "*Fast*-TFM—Multifrequency phasor measurement for distribution networks," *IEEE Trans. Instrum. Meas.*, vol. 67, no. 8, pp. 1825–1835, Mar. 2018.

[19] M. Bertocco, G. Frigo, G. Giorgi, and C. Narduzzi, "Frequency tracking for efficient phasor measurement based on a CSTFM model," in *Proc. IEEE Int. Workshop Appl. Meas. Power Syst. (AMPS)*, Sep. 2015, pp. 84–89.

[20] G. Frigo, G. Giorgi, M. Bertocco, and C. Narduzzi, "Multifunction phasor analysis for distribution networks," in *Proc. IEEE Int. Workshop Appl. Meas. Power Syst. (AMPS)*, Sep. 2016, pp. 1–6.

[21] Y. Zuo, G. Frigo, A. Derviškadic, and M. Paolone, "Impact of synchrophasor estimation algorithms in ROCOF-based under-frequency load-shedding," *IEEE Trans. Power Syst.*, vol. 35, no. 2, pp. 1305–1316, Mar. 2020.

[22] G. Frigo, P. A. Pegoraro, and S. Toscani, "Compressive sensing Taylor-Fourier and windowing approach for synchronized phasor, frequency and ROCOF measurements," in *Proc. IEEE 11th Int. Workshop Appl. Meas. Power Syst. (AMPS)*, Sep. 2021, pp. 1–6.

[23] R. G. Lyons, *Understanding Digital Signal Processing*, 1st ed., Boston, MA, USA: Addison-Wesley, 1996.

[24] D. L. Donoho and X. Huo, "Uncertainty principles and ideal atomic decomposition," *IEEE Trans. Inf. Theory*, vol. 47, no. 7, pp. 2845–2862, Nov. 2001.

[25] M. Elad and A. M. Bruckstein, "A generalized uncertainty principle and sparse representation in pairs of bases," *IEEE Trans. Inf. Theory*, vol. 48, no. 9, pp. 2558–2567, Sep. 2002.

[26] D. Belega and D. Petri, "Frequency estimation by two-or three-point interpolated Fourier algorithms based on cosine windows," *Signal Process.*, vol. 117, pp. 115–125, Dec. 2015.

[27] K. Duda, T. P. Zieliński, and S. Barczentewicz, "Perfectly flat-top and equiripple flat-top cosine windows," *IEEE Trans. Instrum. Meas.*, vol. 65, no. 7, pp. 1558–1567, Jul. 2016.

[28] A. Derviškadić, P. Romano, and M. Paolone, "Iterative-interpolated DFT for synchrophasor estimation: A single algorithm for P- and M-class compliant PMUs," *IEEE Trans. Instrum. Meas.*, vol. 67, no. 3, pp. 547–558, Mar. 2018.

Guglielmo Frigo (Member, IEEE) was born in Padua, Italy, in 1986. He received the B.Sc. and M.Sc. degrees in biomedical engineering from the University of Padova, Padua, in 2008 and 2011, respectively, and the Ph.D. degree from the School of Information Engineering, University of Padova, in 2015, with a dissertation about compressive sensing (CS) theory applications to instrumentation and measurement scenario.

He was a Post-Doctoral Researcher with the Electronic Measurement Research Group, University of Padova, from 2015 to 2017, and the Distributed Electrical Laboratory, Swiss Federal Institute of Technology of Lausanne, Lausanne, Switzerland, from 2018 to 2020. In 2020, he was a Foreign Guest Researcher with the National Institute of Standards and Technology, Gaithersburg, MD, USA. He is currently a Scientist with METAS, Wabern bei Bern, Switzerland. His current research interest includes the development of enhanced measurement infrastructures for electrical systems.

Paolo Attilio Pegoraro (Senior Member, IEEE) received the M.S. *(summa cum laude)* degree in telecommunication engineering and the Ph.D. degree in electronic and telecommunication engineering from the University of Padova, Padua, Italy, in 2001 and 2005, respectively.

From 2015 to 2018, he was an Assistant Professor with the Department of Electrical and Electronic Engineering, University of Cagliari, Cagliari, Italy, where he is currently an Associate Professor. He has authored or coauthored over 130 scientific articles. His current research interests include the development of new measurement techniques for modern power networks, with attention to synchronized measurements and state estimation.

Dr. Pegoraro is a member of IEEE IMS TC 39 (Measurements in Power Systems) and IEC TC 38/WG 47. He is also an Associate Editor of the IEEE TRANSACTIONS ON INSTRUMENTATION AND MEASUREMENT.

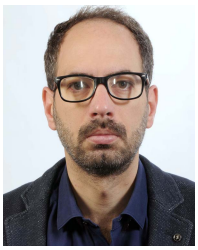

Sergio Toscani (Senior Member, IEEE) received the M.Sc. and Ph.D. degrees *(cum laude)* in electrical engineering from the Politecnico di Milano, Milan, Italy, in 2011.

From 2011 to 2020, he was an Assistant Professor in electrical and electronic measurement with the Dipartimento di Elettronica, Informazione e Bioingegneria, Politecnico di Milano, where he is currently an Associate Professor. His research activity is mainly focused on the development and testing of current and voltage transducers, measurement techniques for power systems, electrical components, and system diagnostics.

Dr. Toscani is a member of the IEEE Instrumentation and Measurement Society and the IEEE TC-39—Measurements in Power Systems.